

THERMAL RADIATION ABSORPTION IN
RECTANGULAR-GROOVE CAVITIES

by E. M. Sparrow

V. K. Jonsson

Heat Transfer Laboratory

Department of Mechanical Engineering

University of Minnesota

Minneapolis 14, Minnesota

**CASE FILE
COPY**

This research was sponsored by the National Aeronautics
and Space Administration (Grant NsG 137-61) under the
technical supervision of Mr. S. Lieblein, Chief, Flow
Processes Branch of the NASA Lewis Research Center.

ABSTRACT

The amount of energy absorbed when a stream of external radiation enters a rectangular-groove cavity has been calculated for a variety of surface conditions, cavity depths, and incident energy distributions. The surfaces of the cavity are either diffuse reflectors or specular reflectors, and a wide range of reflectivity values have been considered. The incoming radiation is either diffusely distributed across the cavity opening or else, arrives in a bundle of parallel rays. As a function of these parameters, results are reported in terms of an apparent absorptivity, which is the ratio of the energy absorbed in the cavity to that which enters. The results show that for diffuse incoming radiation, a specular cavity absorbs more effectively than does a diffuse cavity. For incoming radiation in a parallel ray bundle, the comparison depends on the angle of inclination of the rays.

NOMENCLATURE

- A surface area
- B rate of radiant flux leaving unit surface area, radiosity
- D, E constants of integration
- e₁ rate of diffuse radiation per unit area of opening
- F angle factor
- G, H constants of integration
- H rate of incident energy per unit surface area
- h cavity width
- K₁, K₂ numerical constants, eq. (18)
- k number of surface contacts
- L cavity depth
- L_i directly-illuminated depth

- p exponents
- Q overall rate of energy absorbed
- q local rate of energy absorbed per unit area
- S energy rate per unit area normal to ray
- T_i equivalent temperature of black surface, $e_i = \sigma T_i^4$
- X dimensionless coordinate, x/L
- x distance from cavity opening
- Ξ separation point for k and $k-l$ surface contacts
- Y dimensionless coordinate, y/L
- y distance from cavity opening
- α surface absorptivity
- α_a apparent absorptivity of cavity
- β dimensionless radiosity, B/e_i or $B/S \sin \gamma$
- γ inclination angle, fig. 1
- λ_1, λ_2 numerical constants, eq. (18)
- ξ distance, $|X - Y|$
- ρ reflectivity, $1 - \alpha$
- σ Stefan-Boltzmann constant

INTRODUCTION

This paper is concerned with the energy absorbed when radiation from an external source enters a rectangular-groove cavity. It is well-known that the energy absorbed within any cavity is greater than that which would be absorbed by a plane area stretched tightly over the opening of the cavity. This is called cavity effect and may be explained in terms of the additional opportunities for energy absorption which accompany the multi-reflections within the cavity. The quantitative extent of the cavity effect depends on the shape of the cavity, as well as on the reflecting properties of the surface and on the nature of the incoming energy.

The aim of this investigation is to quantitatively determine the cavity effect for the rectangular groove. The analysis is extended over a wide range of conditions which include surface reflectivity properties, nature of incoming radiation, and groove aspect ratio. Consideration is given to surfaces which may reflect either diffusely (i.e., according to Lambert's Cosine Law) or specularly (angle of incidence equals angle of reflection). For each one of these reflectivity characteristics, consideration is given to radiation which enters the cavity either as a diffuse stream or as a bundle of parallel rays. For these various cases, energy absorption results are obtained and reported as a function of surface absorptivity, groove aspect ratio, and inclination angle of the parallel ray bundle.

A schematic diagram of the rectangular-groove cavity is shown in figure 1 along with dimensional nomenclature. The depth of the groove is measured by L , while the width is h . The length of the cavity in the direction normal to the plane of the figure is sufficiently great so that end effects are negligible. In the case of a parallel ray bundle entering the cavity, the angle γ is used to specify the inclination of the rays to the normal.

It will be convenient to give separate consideration to the cases where the incoming energy is diffusely distributed or arrives in a bundle of parallel

rays. The former will be treated first and the latter second. Separate treatment will also be given for diffusely-reflecting and specularly-reflecting surfaces.

DIFFUSE INCOMING ENERGY, DIFFUSE SURFACES

The stream of diffuse incoming energy is uniformly distributed over the opening of the cavity and may be characterized by e_i per unit area of the opening. For purposes of analysis, the condition of diffuse incoming energy is exactly equivalent to that provided by a plane black surface of emissive power e_i and temperature T_i ($e_i = \sigma T_i^4$) stretched tightly over the cavity opening and radiating into the cavity.

Consideration is first given to the case where the walls of the cavity are diffusely reflecting. The first step in the analysis is to write a radiant flux balance at an area dA_{x_0} (see figure 1) located at a typical position x_0 . Setting aside the contribution of emission,* the energy leaving dA_{x_0} is simply the reflected portion of the incident energy. Denoting the energy leaving a surface location per unit time and area by the radiosity B , and the incident energy per unit time and area by H , we can write

$$B(x_0) = (1 - \alpha) H(x_0) \quad (1)$$

where α is the absorptivity and $F = (1 - \alpha)$ is the reflectivity. The energy incident at x_0 arrives via two paths: (a) directly from the external source and (b) indirectly due to energy reflected at the other surfaces of the cavity. From the external source, there is incident per unit area at x_0

$$e_i F_{x_0-i} \quad (2a)$$

where F_{x_0-i} is an angle factor representing the fraction of the energy leaving

* Energy from an external source enters the cavity, and it is desired to know the amount which is ultimately absorbed. With this in mind, it is only necessary to consider the radiant interchange process for energy which originated at the external source, and energy emitted by the surface need not be considered.

dA_{x_0} which arrives at the surface is stretched across the cavity opening. From a typical position x (area dA_x) on the surface of the cavity, there is incident per unit area at x_0

$$B(x) dF_{x_0 - x} \quad (2b)$$

where $dF_{x_0 - x}$ is the fraction of the energy leaving dA_{x_0} which arrives at dA_x . However, dA_{x_0} receives radiation from all surface locations within its range of visibility, and the total contribution is obtained by integrating expression (2b).

Thus, with equations (2a) and (2b) for the incident energy, the radiant flux balance (1) becomes

$$B(x_0) = (1-\alpha) \left[e_i F_{x_0 - i} + \int_x B(x) dF_{x_0 - x} \right] \quad (3)$$

By inspection of this equation, it may be noted that the unknown B appears under the integral sign as well as in other parts of the equation. Equation (3) is therefore an integral equation.

Once solutions for the radiosity B are available, the energy absorbed in the cavity can be calculated. First, the rate q at which energy is locally absorbed (per unit area) is simply found by multiplying the incident energy H by the absorptivity,

$$q = \alpha H = \frac{\alpha}{1-\alpha} B \quad (4)$$

where equation (1) has been used. Next, the total rate Q at which energy is absorbed in the cavity as a whole may be obtained by integrating equation (4) over the surface of the cavity. For a unit length in the direction normal to figure 1,

$$Q = \frac{2\alpha}{1-\alpha} \int_0^{L+\frac{1}{2}h} B dx \quad (5a)$$

where, due to symmetry, the integral is extended over only half the surface and a factor of two has been included. It is convenient to report the results in terms of an apparent absorptivity α_a defined as

$$\alpha_a = (\text{total absorbed energy}) / (\text{total incoming energy}) \quad (6)$$

Noting that the energy entering the enclosure per unit length normal to the plane of figure 1 is $e_i h$, the apparent absorptivity may be evaluated utilizing

equation (5) as

$$\alpha_a = \frac{2\alpha}{1-\alpha} \int_0^{\frac{L}{h} + \frac{1}{2}} \beta dx \quad (5a)$$

where $\beta = B/e_i$ and $X = x/L$. It is thus seen that the solution of the integral equation (3) holds the key to the determination of the apparent absorptivity.

In approaching the solution of this integral equation, it is advantageous first to simplify its form. Noting that energy leaving dA_{x_0} must either strike the other surfaces of the cavity or else pass out through the opening, it follows that

$$F_{x_0=1} + \int_x dF_{x_0=x} = 1$$

Introducing this into the integral equation (3) and rearranging, there is obtained

$$B'(x_0) = \alpha e_i + (1-\alpha) \int_x B'(x) dF_{x_0=x} \quad (7)$$

where

$$B' = e_i - B, \text{ or } \beta = 1 - (B'/e_i) \quad (7a)$$

But, the integral equation for B' is precisely that which describes the emission problem for a cavity having gray, diffuse walls which are at a uniform temperature T_i ($e_i = \sigma T_i^4$). Moreover, solutions for the emission problem are already available (reference 1), and these may be carried over to the absorption problem being considered here by application of the simple relationship indicated in equation (7a).

The emission solutions covered the range of cavity aspect ratios L/h from 0.25 to 10 for surface absorptivity values α of 0.5, 0.75, and 0.9. Results for the apparent absorptivity α_a corresponding to these conditions have been calculated by application of equation (5a). Utilizing these, α_a values have been graphically interpolated to good accuracy for $\alpha = 0.7$, in order to provide comparisons with later results of this paper. The apparent absorptivities thus obtained have been plotted on figure 2 as a function of cavity aspect ratio for parametric values of the surface absorptivity.

Inspection of the figure reveals that for cavities which are not too deep, the apparent absorptivity increases with increasing depth of cavity. However, for

sufficiently deep cavities, the apparent absorptivity becomes independent of any further increases in depth. The depth of cavity required to achieve the limiting value of apparent absorptivity decreases as the surface absorptivity increases. For instance, for $\alpha = 0.9$, the limiting α_a value (0.976) is essentially achieved at $L/h = 2.5$; while for $\alpha = 0.5$, a hole depth $L/h = 7$ is required to essentially achieve the limiting value of α_a (0.850).

These findings are made plausible by considering the nature of the diffuse reflection process. The energy density of diffusely reflected radiation is the same in all directions. Therefore, some of the energy reflected at each surface contact passes outward through the opening of the cavity, regardless of the depth of the cavity. It is for this reason that all of the energy entering the cavity cannot be fully absorbed.

In appraising the results, it may be noted that in the absence of the cavity effect, α_a would be identically equal to α . Thus, the increase of α_a relative to α is a measure of the magnitude of the cavity effect. The results of figure 2 indicate that the cavity effect is most pronounced for deep cavities and for surfaces of low absorptivity. Thus, utilizing a diffuse cavity having an aspect ratio $L/h \approx 7$, a 70% increase in the effective absorbing power can be achieved relative to a plane surface of absorptivity 0.5. Moreover, a 60% increase can be achieved with a cavity whose aspect ratio is only 1.8!

DIFFUSE INCOMING ENERGY, SPECULAR SURFACES

Consideration is now extended to a cavity whose surfaces are specular reflectors on which the angle of reflection equals the angle of incidence. It will be convenient to replace the incoming diffuse radiation by a black surface of emissive power e_1 . With this, there is formed a complete enclosure composed of the three specular walls of the cavity (designated as 1, 2, and 3) and the black surface (designated as 4). A schematic diagram of the enclosure is shown in figure 3.

One approach toward solving for the radiant interchange within the enclosure would be to keep account of individual rays as they reflect and re-reflect on the specular surfaces. Fortunately, this arduous task may be circumvented by applying a new formulation (reference 2) which utilizes a basic property of images which are formed in plane mirrors. Namely, that light or radiant energy reflected from a plane mirror appears to come from an image which is located behind the mirror, the distance between the image and the mirror being the same as the distance between the object and the mirror.

The development of the new calculation method is described in the reference, and only its application to the absorption problem in the rectangular cavity will be discussed here. Considering figure 3, it is easy to see that the energy absorbed at the cavity walls is equal to the difference between the energy emitted by the black surface and that which is absorbed by it. The energy emitted per unit length normal to the plane of the figure is $e_i h$. Then, denoting by H_4 the energy incident per unit time and area on the black surface, it follows that the rate Q at which energy is absorbed in the cavity as a whole is

$$Q = h [e_i - H_4] \quad (8a)$$

In terms of the apparent absorptivity α_a defined by equation (6), this becomes

$$\alpha_a = 1 - (H_4/e_i) \quad (8b)$$

It is thus seen that the apparent absorptivity will be determined as soon as the incident energy H_4 has been calculated.

In the process of specular reflection by the mirrors 1, 2, and 3, a series of images of surface 4 are formed as indicated in figure 3. The notation may be explained as follows: 4^1 is the image of surface 4 formed by one specular reflection, 4^2 is the image formed by two specular reflections, and in general, 4^n is the image formed after n specular reflections. The subscript u refers to upper set of images, while the lower images are without subscripts. Clearly,

since the upper images lie in the same plane as surface \mathbb{h} , energy leaving these images will not impinge directly on surface \mathbb{h} . The radiation leaving a typical lower image surface \mathbb{h}^n per unit area is

$$e_i (1 - \alpha)^n$$

where $(1 - \alpha) = \rho$ is the reflectivity. Of this, an amount

$$e_i (1 - \alpha)^n F_{\mathbb{h} - \mathbb{h}^n} \quad (9a)$$

reaches surface \mathbb{h} , where it is absorbed. The angle factor $F_{\mathbb{h} - \mathbb{h}^n}$ corresponds to diffuse radiation between surfaces \mathbb{h} and \mathbb{h}^n . From all of the image surfaces, there arrives at \mathbb{h}

$$H_4 = e_i \left[(1 - \alpha) F_{\mathbb{h} - \mathbb{h}^1} + 2 \sum_{n=2}^{\infty} (1 - \alpha)^n F_{\mathbb{h} - \mathbb{h}^n} \right] \quad (9b)$$

and with this, the apparent absorptivity may be evaluated from equation (8b) as

$$\alpha_a = 1 - \left[(1 - \alpha) F_{\mathbb{h} - \mathbb{h}^1} + 2 \sum_{n=2}^{\infty} (1 - \alpha)^n F_{\mathbb{h} - \mathbb{h}^n} \right] \quad (10)$$

It only remains to furnish the angle factors $F_{\mathbb{h} - \mathbb{h}^n}$. These may be most easily derived by the method of crossed and uncrossed strings due to Hottel* (reference 3). In this method, strings are imagined to be tightly stretched between the end points of surfaces \mathbb{h} and \mathbb{h}^n . The angle factor is then obtained by summing the lengths of the two crossed strings and subtracting away the lengths of the two uncrossed strings, and then dividing the difference by $2h$. In this way, there is obtained

$$F_{\mathbb{h} - \mathbb{h}^n} = \frac{1}{2} \left[\sqrt{(n-2)^2 + (2L/h)^2} + \sqrt{n^2 + (2L/h)^2} - 2 \sqrt{(n-1)^2 + (2L/h)^2} \right] \quad (11)$$

Inspection of equations (10) and (11) reveals that the apparent absorptivity α_a depends upon two parameters, the cavity aspect ratio L/h and the surface absorptivity α . For each $L/h, \alpha$ combination, the infinite series appearing in equation (11) was summed, and α_a thus obtained. The actual numerical

* This method applies to surfaces which are very long in one direction.

calculations were performed on a Univac 1103 digital computer. The series was truncated when the contribution of a given term was less than 10^{-5} of the sum of the series.

Results for the apparent absorptivity have been plotted on figure 4 as a function of cavity aspect ratio for parametric values of the surface absorptivity. In recognition of the fact that specular surfaces may have higher reflectivity values than diffuse surfaces, lower α values have been included on figure 4. From the figure, it is seen that the apparent absorptivity increases monotonically with increasing cavity depth, ultimately approaching the value of unity for sufficiently deep cavities. This is in contrast to the behavior of diffuse surfaces (figure 2), for which the apparent absorptivity approaches a limiting value less than unity for very deep cavities. These contrasting findings may be understood by taking cognizance of the different nature of the two reflection processes. In the case of diffuse reflection, a portion of the energy reflected at each surface contact passes outward through the cavity opening. In the case of specular reflection, only energy which reaches the bottom of the cavity and is reflected from the base surface 3 (figure 3) can ever pass outward through the cavity opening. Thus, for sufficiently deep specular cavities, essentially all of the incoming radiation is absorbed. It is also easily understood that deeper cavities are needed to achieve the total absorption condition for surfaces of lower absorptivity.

It is interesting to compare the absorbing power of diffuse and specular cavities for diffuse incoming radiation. Comparing corresponding curves on figures 2 and 4, it is seen that a specular cavity absorbs more effectively than does a diffuse cavity. The advantages of the specular cavity are accentuated for deep cavities and for low surface absorptivities. For example, for $\alpha = 0.5$, the apparent absorptivity values for specular and diffuse surfaces at $L/h = 1$ are

0.762 and 0.742. At $L/h = 10$, the corresponding values are 0.963 and 0.850.

A similar comparison shows smaller deviations for $\alpha = 0.9$.

PARALLEL INCOMING RAYS, DIFFUSE SURFACES

When a parallel ray bundle enters the cavity under an inclination angle γ , a length L_i of one cavity wall is directly illuminated as shown in the inset of figure 5. From the geometry of the figure,

$$L_i = h/\tan \gamma \quad (12)$$

The remainder of the cavity walls receives radiation only by reflection. Different quantities of energy will thus be incident on oppositely-located positions on the parallel walls of the cavity. In cognizance of this lack of symmetry, separate coordinates x and y are employed to specify positions on the parallel walls, see figure 5.

When the surfaces of the cavity are diffuse reflectors, the radiant interchange within the cavity is described by integral equations. Because of the asymmetry noted above, several integral equations are required. Additionally, the solutions of these integral equations will depend on three independent parameters: the aspect ratio L/h , the surface absorptivity α , and the inclination angle γ of the incoming rays. A complete set of solutions to this problem involving several simultaneous integral equations and three independent parameters is a very formidable computational undertaking, especially since numerical means must be utilized. Now, in the previous case of diffuse incoming energy and diffuse surfaces, it was found that cavities of moderate depth displayed absorption characteristics very little different from those of a cavity of infinite depth. Taking cognizance of this, it was decided to reduce the number of parameters in the present problem of incoming parallel rays by focusing attention on the cavity of infinite depth. Such a cavity is shown in the inset of figure 5. Approximate auxiliary calculations were carried out to determine the depth of the finite cavity for which the infinite cavity results would apply.

The mathematical formulation of the problem follows parallel to that which has been carried out for the case of diffuse incoming energy. The radiant flux balance of equation (1) continues to apply. It remains to evaluate the incident energy H . If the energy carried by the parallel ray bundle is denoted by S per unit time and area normal to the ray, then

$$S \sin \gamma \quad (13)$$

is the rate at which external energy is incident per unit area of surface in the range $0 \leq x \leq L_1$. On all other regions of the cavity surface, the direct incidence of external radiation is zero. The contribution to H of radiation reflected from the surface of the cavity is obtained by integrating expressions having the form of equation (2b). Thus, we can write

$$B(x) = (1 - \alpha) \left[S \sin \gamma + \int_{y=0}^{\infty} B(y) dF_{x-y} \right] \quad 0 < x < L_1 \quad (14a)$$

$$B(x) = (1 - \alpha) \left[\int_{y=0}^{\infty} B(y) dF_{x-y} \right] \quad L_1 < x \leq \infty \quad (14b)$$

$$B(y) = (1 - \alpha) \left[\int_{x=0}^{\infty} B(x) dF_{y-x} \right] \quad 0 \leq y \leq \infty \quad (14c)$$

To complete the formulation, it is necessary to derive the angle factors. For the case where the surfaces are very long in the direction normal to the plane of the figure, there is a particularly simple method for finding angle factors which is based on equation (31-58) of reference 4. For instance, to find dF_{x-y} , the normal is constructed at x and the connecting line is drawn from x to y . The angle included between the normal and the connecting line is denoted by ϕ . Then, applying the differential form of equation (31-58), which states that

$$dF_{x-y} = \frac{1}{2} \frac{d}{dy} (\sin \phi) dy$$

there is obtained

$$dF_{x-y} = \frac{1}{2} \frac{h^2}{[(y-x)^2 + h^2]^{3/2}} dy \quad (15a)$$

A similar expression is found for dF_{y-x} , except that dy is replaced by dx . In terms of dimensionless variables $X = x/h$, $Y = y/h$, the angle factors become

$$dF_{x-y} = \frac{1/2}{[(Y-X)^2 + 1]^{3/2}} dY, \quad dF_{y-x} = \frac{1/2}{[(Y-X)^2 + 1]^{3/2}} dx \quad (15b)$$

The function $[(Y-X)^2 + 1]^{-3/2}$ has been plotted as a solid curve on figure 6, with ξ representing the distance $Y-X$. It is seen that this function has the general form of an exponential. The figure shows that a given surface location is most affected by radiation from other surface locations which are directly across from it, i.e., at small ξ .

A final dimensionless form of the integral equations (14) is obtained by letting

$$\beta = B/S \sin \gamma \quad (16)$$

The effect of this substitution is to replace B by β in all terms of equations (14), and to replace $S \sin \gamma$ by 1.

The numerical solution of equations (14) as a function of two independent parameters is still a formidable computational undertaking. The lengthy digital computer solutions can, however, be circumvented by applying a method first used by Buckley (reference 5) with very good accuracy (reference 6) in connection with the emission problem in circular holes. Later investigators have used Buckley's method for various cases of radiant interchange in circular-cylindrical tubes, but to the knowledge of the authors, this approach has yet to be applied to the rectangular groove. Buckley recognized that the angle factor varied approximately as an exponential function of distance, and he proposed that the actual angle factor be approximated either by a single exponential or by a sum of exponentials.

Following through on this idea for the case of the rectangular groove, one and two term exponential approximations for the angle factor have been derived and are plotted on figure 6. The two term exponential provides a good representation for the angle factor and will be used here.

In incorporating the exponential approximation into the analysis, cognizance must be taken of the fact that ξ represents a distance between points and is therefore intrinsically positive. This means that for $Y < X$, ξ denotes $X - Y$, while for $Y > X$, ξ denotes $Y - X$. This point may be illustrated by evaluating equation (14a) in terms of the exponential angle factor.

$$\beta(X) = (1-\alpha) + (1-\alpha) \int_{y=0}^X \beta(y) [K_1 e^{-\lambda_1(X-y)} + K_2 e^{-\lambda_2(X-y)}] dy \\ + (1-\alpha) \int_{y=X}^{\infty} \beta(y) [K_1 e^{-\lambda_1(Y-X)} + K_2 e^{-\lambda_2(Y-X)}] dy \quad (17)$$

where $K_1 = 1.2465$ $\lambda_1 = 1.203$
 $K_2 = -0.2465$ $\lambda_2 = 6.8157$ (18)

Integral equations similar to (17) can be written for equations (14b) and (14c).

Continuing with the analysis, it is convenient to represent the unknowns by four functions $\beta_1, \beta_2, \beta_3, \beta_4$ as follows

$$\begin{aligned} \beta(X) &= \beta_1(X), & 0 \leq X < L_i/h \\ \beta(X) &= \beta_2(X), & L_i/h < X \leq \infty \\ \beta(Y) &= \beta_3(Y), & 0 \leq Y < L_i/h \\ \beta(Y) &= \beta_4(Y), & L_i/h < Y \leq \infty \end{aligned} \quad (19)$$

The next step is to reduce the governing integral equations to differential equations. This is possible because the X /dependence of exponential functions such as $e^{-\lambda_1(X-Y)}$ and $e^{-\lambda_2(X-Y)}$ is unchanged by differentiation. In recognition of this, equation (17) is differentiated four times with respect to X .

Then, by properly combining equation (17) with the second and fourth derivatives, it is found that all the terms containing integrals cancel out, leaving

$$\begin{aligned}\beta_1''' &= (\lambda_1^2 + \lambda_2^2) \beta_1'' + \lambda_1^2 \lambda_2^2 \beta_1 - (1-\alpha)(K_1 \lambda_1 + K_2 \lambda_2) \beta_4'' \\ &\quad - (1-\alpha) \lambda_1^2 \lambda_2^2 \beta_4 = (1-\alpha) \lambda_1^2 \lambda_2^2\end{aligned}\quad (20)$$

where the primes denote differentiation. In a similar way, differentiation of equation (18c) with respect to Y , $0 \leq Y \leq L_i/h$, yields

$$\begin{aligned}\beta_4''' &= (\lambda_1^2 + \lambda_2^2) \beta_4'' + \lambda_1^2 \lambda_2^2 \beta_4 - (1-\alpha)(K_1 \lambda_1 + K_2 \lambda_2) \beta_1'' \\ &\quad - (1-\alpha) \lambda_1^2 \lambda_2^2 \beta_1 = 0\end{aligned}\quad (21)$$

It is seen that equations (20) and (21) are a pair of simultaneous, linear, fourth-order, ordinary differential equations for the functions β_1 and β_4 . The homogeneous part* of such equations must have exponential solutions

$$\beta_1 = E e^{pX}, \quad \beta_4 = D e^{pY} \quad (22)$$

Introducing these into the homogeneous part of the differential equations (20) and (21) yields two linear, homogeneous, algebraic equations for E and D with coefficients which contain p , λ_1 , λ_2 , K_1 , and K_2 . A non-trivial solution to these homogeneous algebraic equations is possible only if the determinant of the coefficients is zero. This yields a polynomial of eight degree (the so-called secular equation) for the exponent p , for which it is found that there are eight real roots. These roots pair off together as follows: $\pm p_1, \pm p_2, \pm p_3, \pm p_4$. A listing of the expressions for p_1, p_2, p_3 , and p_4 is given in the Appendix.

Returning to the linear algebraic equations, it is additionally found that

$$\begin{aligned}D_i &= E_i, \quad \text{for } i = 1, 2, 3, 4 \\ D_i &= -E_i, \quad \text{for } i = 5, 6, 7, 8\end{aligned}$$

Therefore, with this information, the solutions for β_1 and β_4 can be written.

* right-hand sides equal zero.

$$\beta_1 = E_0 + E_1 e^{P_1 X} + E_2 e^{P_2 X} + E_3 e^{-P_1 X} + E_4 e^{-P_2 X} + E_5 e^{P_3 X} + E_6 e^{P_4 X} \\ + E_7 e^{-P_3 X} + E_8 e^{-P_4 X} \quad (22a)$$

$$\beta_4 = D_0 + E_1 e^{P_1 Y} + E_2 e^{P_2 Y} + E_3 e^{-P_1 Y} + E_4 e^{-P_2 Y} - E_5 e^{P_3 Y} - E_6 e^{P_4 Y} \\ - E_7 e^{-P_3 Y} - E_8 e^{-P_4 Y} \quad (22b)$$

where E_0 and D_0 are the particular solutions.

Proceeding along the same lines indicated in the preceding paragraph, the integral equations for β_2 and β_3 can be reduced to differential equations. Both of these differential equations have precisely the form of equation (21), with β_4 and β_1 respectively replaced by β_2 and β_3 or by β_3 and β_2 . Solutions for this pair of simultaneous, linear, homogeneous differential equations are

$$\beta_2 = G e^{pX}, \quad \beta_3 = H e^{pY} \quad (23)$$

Substituting these into the differential equations leads to a pair of linear, homogeneous algebraic equations which give eighth roots for $p: \pm p_1, \pm p_2, \pm p_3, \pm p_4$ and also that

$$H_i = G_i, \quad i = 1, 2, 3, 4$$

$$H_i = -G_i, \quad i = 5, 6, 7, 8$$

With this information, the solutions for β_2 and β_4 may be written as

$$\beta_2 = G_3 e^{-p_1 X} + G_4 e^{-p_2 X} + G_7 e^{-p_3 X} + G_8 e^{-p_4 X} \quad (23a)$$

$$\beta_4 = G_3 e^{-p_1 Y} + G_4 e^{-p_2 Y} - G_7 e^{-p_3 Y} - G_8 e^{-p_4 Y} \quad (23b)$$

The constants G_1, G_2, G_5 , and G_6 are multipliers of terms such as $e^{p_1 X}, e^{p_2 X}$, etc.

These exponentials approach infinity as X and Y approach infinity. Therefore,

to satisfy the condition that β_2 and β_3 are everywhere finite

$$G_1 = G_2 = G_5 = G_6 = 0 \quad (24)$$

To complete the solution, it only remains to determine the constants of integration which appear in equations (22a), (22b), (23a), and (23b). These may be found by returning to the four integral equations of the problem and introducing the solutions for β_1 , β_2 , β_3 , and β_4 as given by equations (22a), (22b), (23a), and (23b). After the integrations are carried out, terms are grouped according to the exponential (e.g., e^{1X} , e^{2X} , etc.) which multiplies them. In this way, there are obtained 14 linear algebraic equations for the 14 unknown constants. These equations are solvable in closed form, and the final expressions are given in the Appendix. By inspection of these expressions, it is seen that the solutions depend upon the surface absorptivity α and the inclination angle γ of the incident rays.

With the solution for the radiosity B now at hand, consideration can be given to the energy absorbed in the cavity. The local rate of energy absorption per unit area is given by equation (4). Substituting the current definition of β from equation (16), the expression for q becomes

$$q = \left[\frac{\alpha}{1-\alpha} S \sin \gamma \right] \beta \quad (25)$$

The rate of energy absorption in the cavity as a whole can be obtained by integrating equation (25) along both walls of the cavity. Then, noting that the total rate of incoming energy is $(S \sin \gamma) L_1$, the apparent absorptivity α_a can be evaluated from its definition (6) as

$$\alpha_a = \frac{\alpha \tan \gamma}{1-\alpha} \left[\int_0^\infty \beta(X) dX + \int_0^\infty \beta(Y) dY \right] \quad (26)$$

where h/L_1 has been replaced by $\tan \gamma$ according to equation (12). The solutions for β as given by equations (22a), (22b), (23a), and (23b) may then be introduced,

and after the indicated integration is carried out, there is obtained

$$\alpha_a = \frac{2\alpha \tan \gamma}{1-\alpha} \left[\frac{D_0 + E_0}{2 \tan \gamma} + \frac{E_1}{P_1} (e^{-P_1 \cot \gamma} - 1) + \frac{E_2}{P_2} (e^{-P_2 \cot \gamma} - 1) - \frac{E_3}{P_1} (e^{-P_1 \cot \gamma} - 1) - \frac{E_4}{P_2} (e^{-P_2 \cot \gamma} - 1) + \frac{G_3}{P_1} e^{-P_1 \cot \gamma} + \frac{G_4}{P_2} e^{-P_2 \cot \gamma} \right] \quad (26a)$$

Utilizing equation (26a) in conjunction with the expressions for p , D , E , and G as given in the Appendix, the apparent absorptivity has been evaluated for inclination angles γ ranging from 10° to 80° and for surface absorptivities α ranging from 0.3 to 0.9. These results are plotted in figure 5. From the figure, it is seen that the apparent absorptivity is greater as the inclination angle γ decreases. This finding is made plausible by noting that the external radiation penetrates more deeply into the cavity as γ decreases and must therefore undergo many diffuse reflections before appreciable amounts can escape. Thus, for ray bundles which arrive at deep diffuse cavities under small angles of inclination, there is a very appreciable cavity effect. As before, the cavity effect is accentuated with decreasing surface absorptivity.

It is interesting to inquire as to whether the diffuse-surfaced cavity absorbs more effectively if the incoming energy is in a parallel ray bundle or is diffusely distributed. For deep cavities, this information can be obtained by comparing the curves of figure 5 with the horizontal asymptotes of figure 2. From this comparison, it is found that rays which arrive at a small inclination angle γ are more fully absorbed than is diffuse incoming energy. The contrary is true for rays which arrive under a large inclination angle. These findings may be illuminated by noting that a ray bundle arriving at a small inclination angle penetrates deeply into the cavity; substantially deeper than the diffuse incoming stream. For a ray bundle arriving at a large inclination angle, the opposite is true. Further inspection of figures 2 and 5 reveals that when $\gamma \approx 30^\circ$, the two types of incoming radiation are absorbed about equally well.

The results of figure 5 were obtained from an analysis for the cavity of infinite depth. However, as already indicated, these results should also apply to finite cavities of sufficient depth. An approximate calculation was performed to determine the depth of finite cavity to which the infinite cavity results would apply to within 2%. These calculations were carried out by following groups of incoming rays as they diffusely reflected and re-reflected within the cavity. Account was kept of the energy absorbed at each surface contact and summation gave the total energy absorbed. For each inclination angle and surface absorptivity, the depth of cavity for which the apparent absorptivity is approximately 98% of that given on figure 5 was found by trial and error. The cavity aspect ratios thus obtained are plotted in figure 7 as a function of inclination angle for parametric values of surface absorptivity. From the figure, it is seen that for cavities with surface absorptivities of 0.5 and larger, only moderate cavity depths are needed to achieve the absorbing power of a cavity of infinite depth. For cavities of lower absorptivity, deeper cavities are required, especially at small inclination angles.

PARALLEL INCOMING RAYS, SPECULAR SURFACES

The analysis for the case of parallel rays incident on a specular cavity may be carried through by a different and basically simpler approach than that given for diffuse surfaces. The derivation is facilitated by reference to figure 8. Here, there is shown a single ray entering the cavity, reflecting on the walls, and then emerging from the opening. A mirror image of the cavity as formed in the base surface is also shown at the left by the dashed lines. Suppose, for the moment, that the base surface is removed and that the ray can move freely through a cavity of length $2L$. Then, the figure demonstrates that the reflection pattern in the dashed (image) portion of this cavity is identical to that which occurs in the actual cavity after the ray has been reflected from the base surface.

Thus, the number of surface contacts which a ray experiences within the actual cavity is equal to the number experienced in a cavity of length $2L$ open at both ends, plus one additional to account for reflection at the base.

The ray which has been constructed in the figure has a special characteristic. Namely, that after making three contacts with the surface, it grazes the cavity wall as it leaves through the opening. Additional study of the figure indicates that rays which initially strike the surface in the region $x < \bar{x}$ will experience four surface contacts within the cavity, while rays which initially strike in the range $x > \bar{x}$ will experience three surface contacts. Thus, \bar{x} divides the surface into two zones, such that rays striking within each zone have a uniform number of surface contacts.

The number of surface contacts k experienced by rays which strike in the region $0 \leq x < \bar{x}$ may be determined from the geometry of figure 8 as

$$k = \text{integral part} [2(L/L_1) + 2] \quad (27)$$

If the quantity in braces is precisely an integer, then k is equal to that integer minus one. For rays which strike the surface in the region $\bar{x} < x \leq L_1$, the number of surface contacts which are experienced within the cavity is $k-1$. Furthermore, from the geometry of the figure, it follows that the dividing point \bar{x} is given by

$$\bar{x}/L_1 = 2(L/L_1) - (k-2) \quad (28)$$

When a ray experiences k contacts with the surface, the fraction of its energy which is thus absorbed is

$$\alpha + \alpha(1-\alpha) + \alpha(1-\alpha)^2 + \dots + \alpha(1-\alpha)^{k-1} \quad (29a)$$

This is a geometric series whose sum is

$$1 - (1-\alpha)^k \quad (29b)$$

With this, we can now calculate the apparent absorptivity α_a from its definition, equation (6). The energy absorbed in the cavity is

$$S \sin \gamma \left\{ \bar{x} [1 - (1-\alpha)^k] + (L_1 - \bar{x}) [1 - (1-\alpha)^{k-1}] \right\} \quad (30)$$

where S denotes the energy per unit area normal to the ray. The rate at which energy enters the cavity is $L_i S \sin \gamma$. Then, introducing this information into equation (6) and taking \bar{x} from equation (28), there is obtained

$$\alpha_a = \left[2 \frac{L}{L_i} - (k-2) \right] \left[1 - (1-\alpha)^k \right] + \left[k-1 - 2 \frac{L}{L_i} \right] \left[1 - (1-\alpha)^{k-1} \right] \quad (31)$$

It is easily verified that this expression is equally valid for $L/L_i < 1$ as well as for $L/L_i \geq 1$.

Consideration may now be given to the computation of numerical results.

From equation (27), it is seen that for $0 < L/L_i \leq 1/2$, $k = \text{constant} = 2$; $1/2 < L/L_i \leq 1$, $k = \text{constant} = 3$; $1 < L/L_i \leq 3/2$, $k = \text{constant} = 4$, and so forth. From this, it is clear that the number of surface contacts increases by one as a length increment $1/2 L_i$ is added. Then, turning to equation (31), it is seen that within a given range such as $0 < L/L_i \leq 1/2$, α_a increases linearly with L/L_i . The same is true in the range $1/2 < L/L_i \leq 1$, except that the slope of α_a versus L/L_i is different (because k is different). Therefore, a graph of α_a is composed of a succession of straight line segments which change slope at $L/L_i = 1/2, 1, 3/2, 2, \dots$

Figure 9 presents results for α_a as a function of L/L_i for parametric values of α . The previously-described changes in slope are clearly evident. From the abscissa, it is seen that L/h and γ do not appear as separate parameters, but rather, combine as the single parameter $(h/L) \tan \gamma$. Taking cognizance of this, it is evident from the figure that a given cavity (i.e., given L/h) absorbs energy more effectively when the rays arrive under a large angle of inclination (i.e., large γ). This is because such rays undergo a greater number of specular reflections than do rays which arrive at a small angle of inclination. This is precisely opposite to the characteristics of diffusely-reflecting cavities, which are more effective absorbers for rays which arrive under a small angle of inclination (see figure 5). Additionally, for rays arriving at a given angle of inclination (given γ), figure 9 indicates that the amount of energy absorbed

increases steadily as the cavity depth increases and ultimately approaches total absorption, i.e., $\alpha_a = 1$. For diffuse surfaces, it may be recalled that complete absorption is not possible regardless of the depth of the cavity.

It is interesting to inquire whether a specular cavity absorbs more effectively when the incoming radiation is a diffuse stream or a parallel ray bundle. From a study of figures 2 and 9, it is found that parallel rays arriving at a large angle of inclination are more strongly absorbed than is diffuse incoming energy. On the other hand, rays arriving under a small angle of inclination are less strongly absorbed than is diffuse energy.

REFERENCES

1. J. L. Grigg, personal communication, report in progress.
2. E. M. Sparrow, E. R. G. Eckert and V. K. Jonsson, "An Enclosure Theory for Radiative Exchange Between Specularly and Diffusely Reflecting Surfaces," ASME paper 61-WA-167. To be published in Trans. ASME, Journal of Heat Transfer.
3. H. C. Hottel, "Radiant Heat Transmission," chapter 4 of "Heat Transmission," by W. H. McAdams, Third edition, McGraw-Hill Book Company, Inc., New York, N. Y., 1954.
4. Max Jakob, "Heat Transfer," vol. 2, John Wiley and Sons, Inc., New York, N. Y., 1957.
5. H. Buckley, "On the Radiation From the Inside of a Circular Cylinder," Philosophical Magazine, vol. 4, no. 23, 1927, pp. 753-762.
6. E. M. Sparrow and L. U. Albers, "Apparent Emissivity and Heat Transfer in a Long Cylindrical Hole," Trans. ASME, Journal of Heat Transfer, vol. 82C, 1960, pp. 253-255.

APPENDIX

Expressions for p, D, E, and G.

$$\left. \begin{array}{l} p_1 \\ p_2 \end{array} \right\} = \sqrt{\frac{\lambda_1^2 + \lambda_2^2 + (1-\alpha)(K_1\lambda_1 + K_2\lambda_2)}{2}} = \sqrt{\frac{[\lambda_1^2 + \lambda_2^2 + (1-\alpha)(K_1\lambda_1 + K_2\lambda_2)]^2 - 4\alpha\lambda_1^2\lambda_2^2}{2}}$$

$$\left. \begin{array}{l} p_3 \\ p_4 \end{array} \right\} = \sqrt{\frac{\lambda_1^2 + \lambda_2^2 - (1-\alpha)(K_1\lambda_1 + K_2\lambda_2)}{2}} = \sqrt{\frac{[\lambda_1^2 + \lambda_2^2 - (1-\alpha)(K_1\lambda_1 + K_2\lambda_2)]^2 - 4(2-\alpha)\lambda_1^2\lambda_2^2}{2}}$$

$$\text{Let } z_1 = \frac{1-\alpha}{\alpha}, \quad z_2 = \frac{1-\alpha}{2-\alpha}$$

$$\text{Then } D_0 = z_1 z_2 \quad E_0 = z_2/\alpha$$

For k = 1, 2, 5, 6

$$E_k = \frac{\frac{z_m}{4} P_i^2 (\lambda_i^2 - P_i^2) (\lambda_j^2 - P_j^2)}{\lambda_i^2 \lambda_j^2} e^{-P_i \cot \gamma}$$

where i, j, and m are given by the following table:

k	i	j	m
1	1	2	1
2	2	1	1
5	3	4	2
6	4	3	2

For k = 3, 4, 7, 8

$$E_k = \frac{\frac{z_m}{4} P_i (P_i + P_j) (P_j + P_i)}{\lambda_i^2 \lambda_j^2} \left[(P_i + P_j) P_j (\lambda_i + P_i) (\lambda_j + P_i) e^{-P_i \cot \gamma} \right. \\ \left. - 2 P_i^2 (\lambda_i + P_i) (\lambda_j + P_j) e^{-P_j \cot \gamma} + 2 (P_i^2 - P_j^2) \lambda_i \lambda_j \right]$$

$$G_K = \frac{z_m p_j (\lambda_i^2 - p_i^2)}{4(p_i - p_j)(p_i^2 - p_j^2) \lambda_i^2 \lambda_j^2} \left[- (p_i + p_j) p_j (\lambda_2^2 - p_i^2) \right. \\ \left. + 2p_i^2 (\lambda_2^2 - p_j^2) - 2(p_i^2 - p_j^2) \lambda_2^2 \right] + E_K$$

where i , j , and m are given by the following table:

k	i	j	m
3	1	2	1
4	2	1	1
7	3	4	2
8	4	3	2

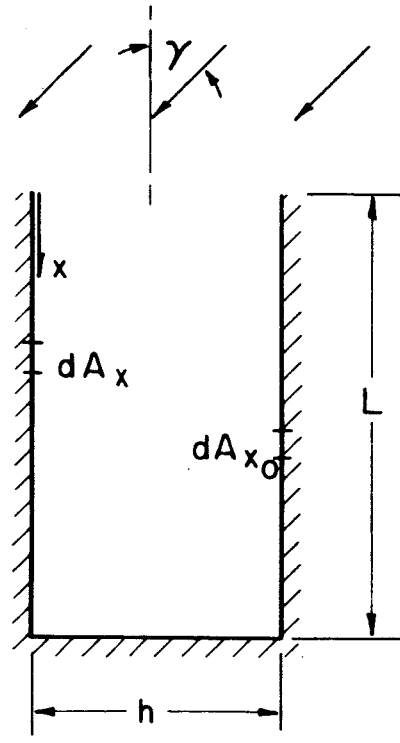


Fig. I Rectangular - Groove Cavity

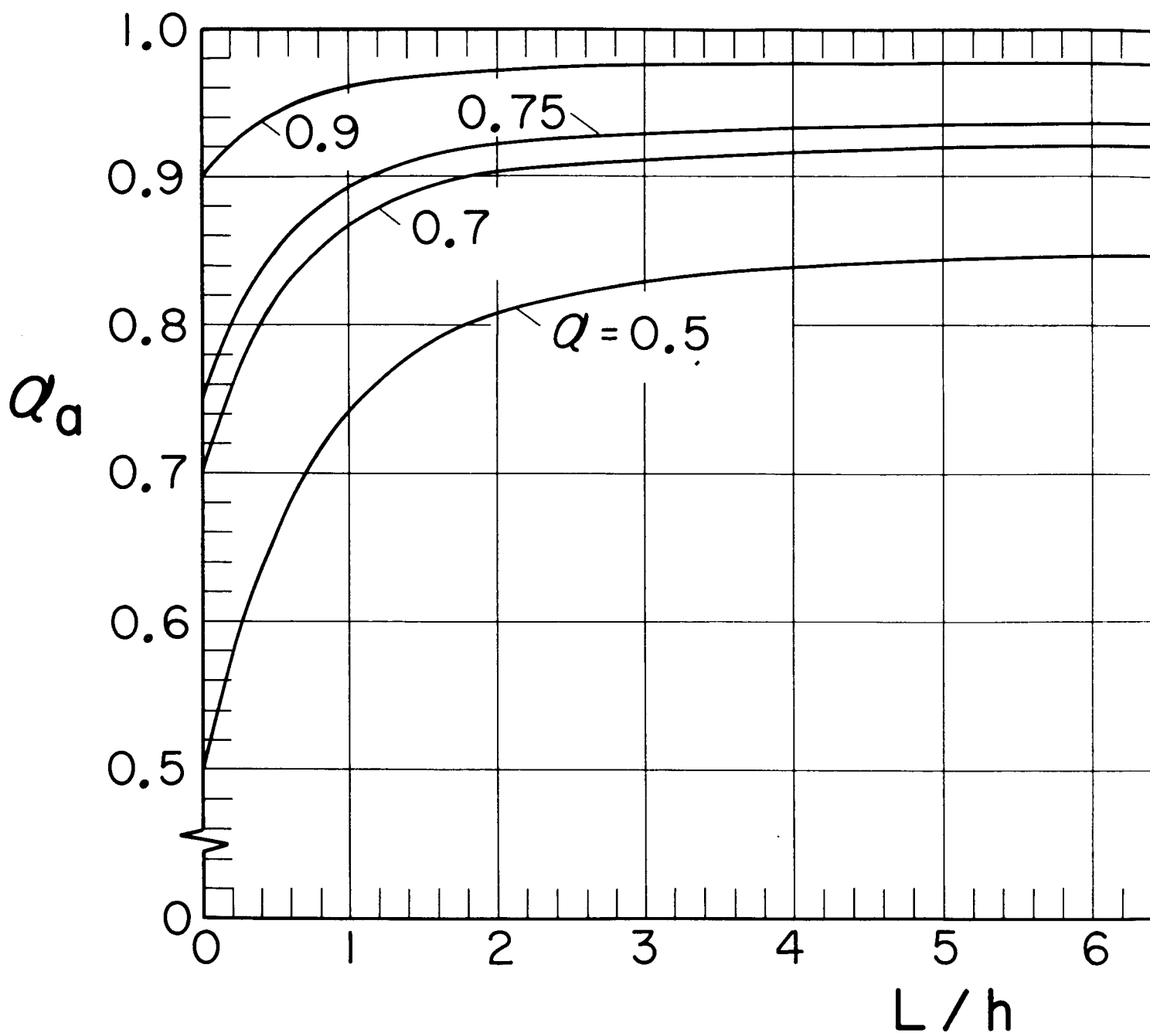
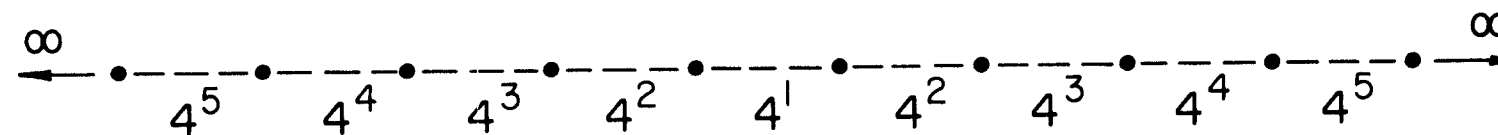
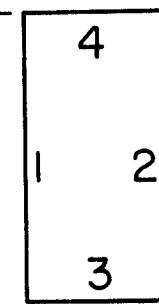
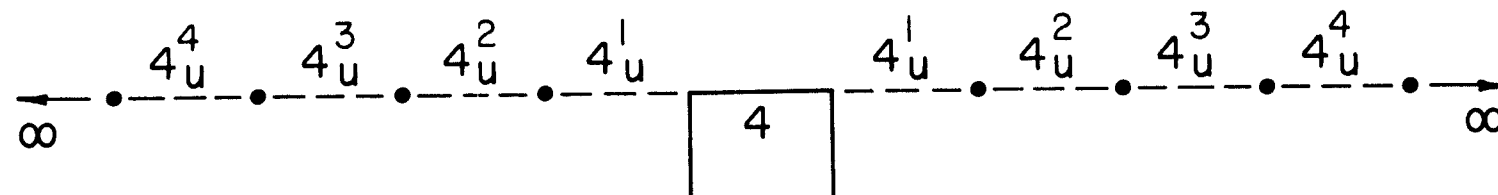


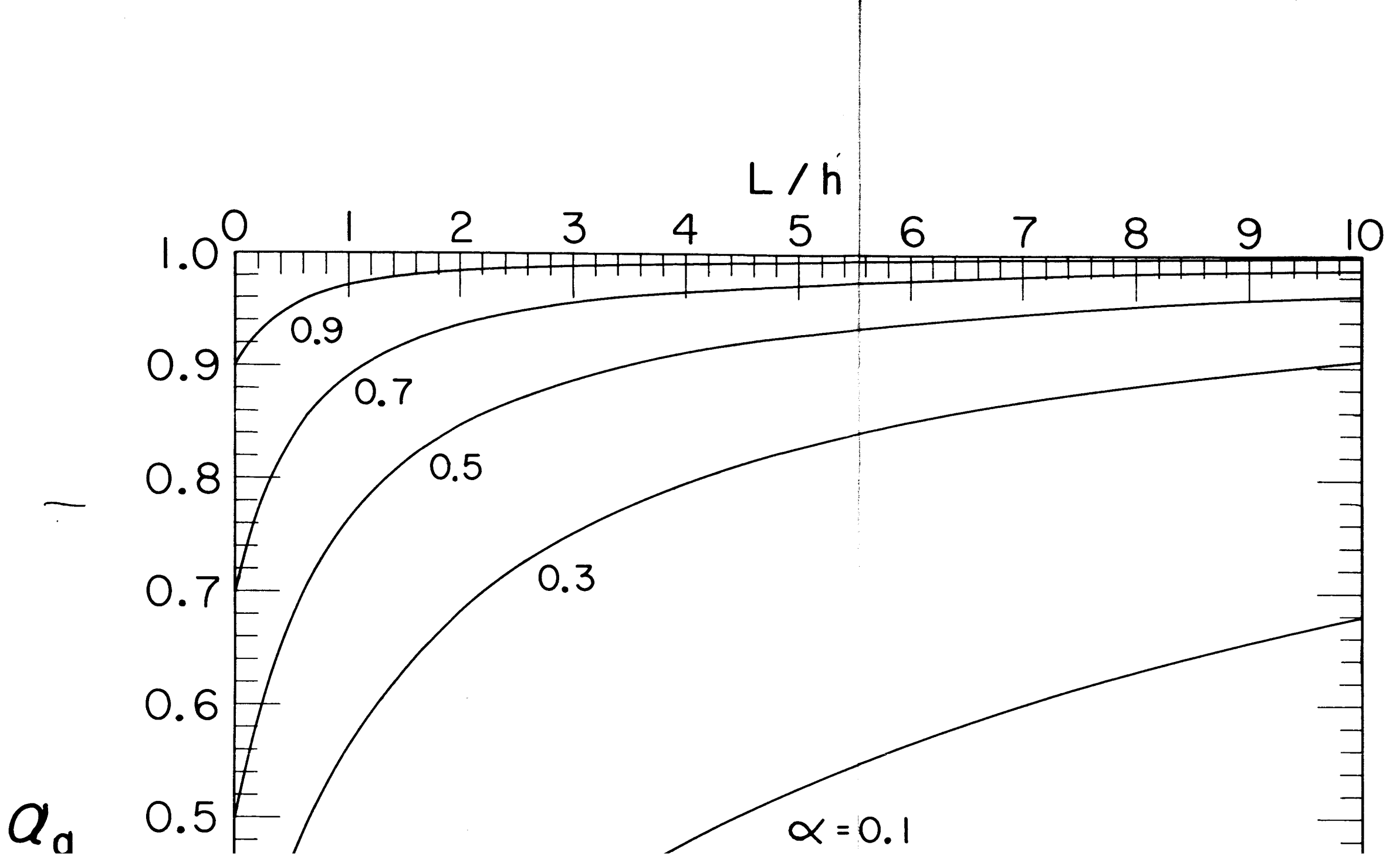
Fig. 2 Apparent Absorptivity for Diffuse Energy Enteri



1, 2, 3: SPECULAR

4: DIFFUSE(BLACK)

Fig.3 Images Formed by Diffuse Incoming Radiation in a Specular Cavity



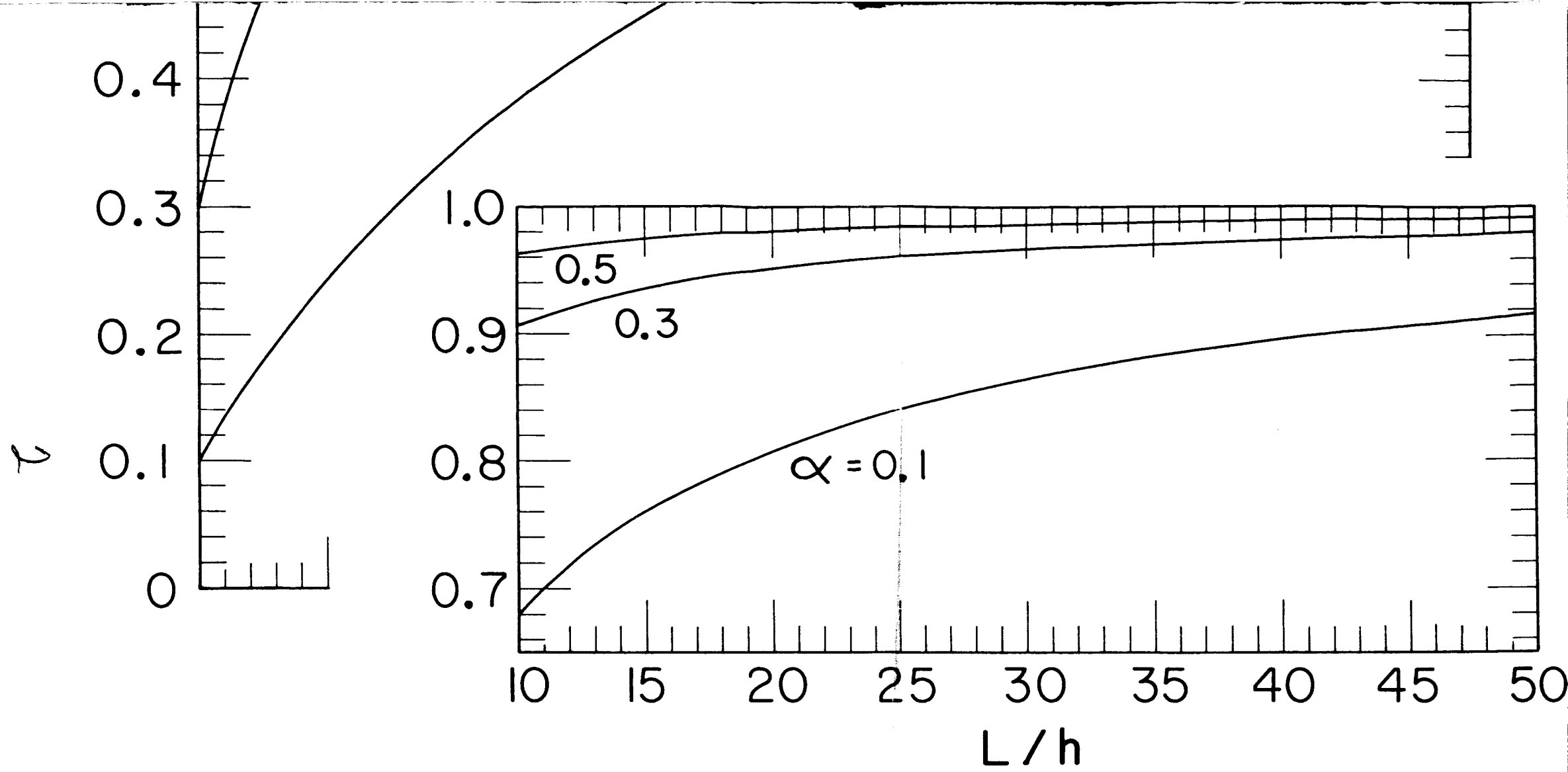


Fig. 4 Apparent Absorptivity for Diffuse Energy Entering a Specular Cavity

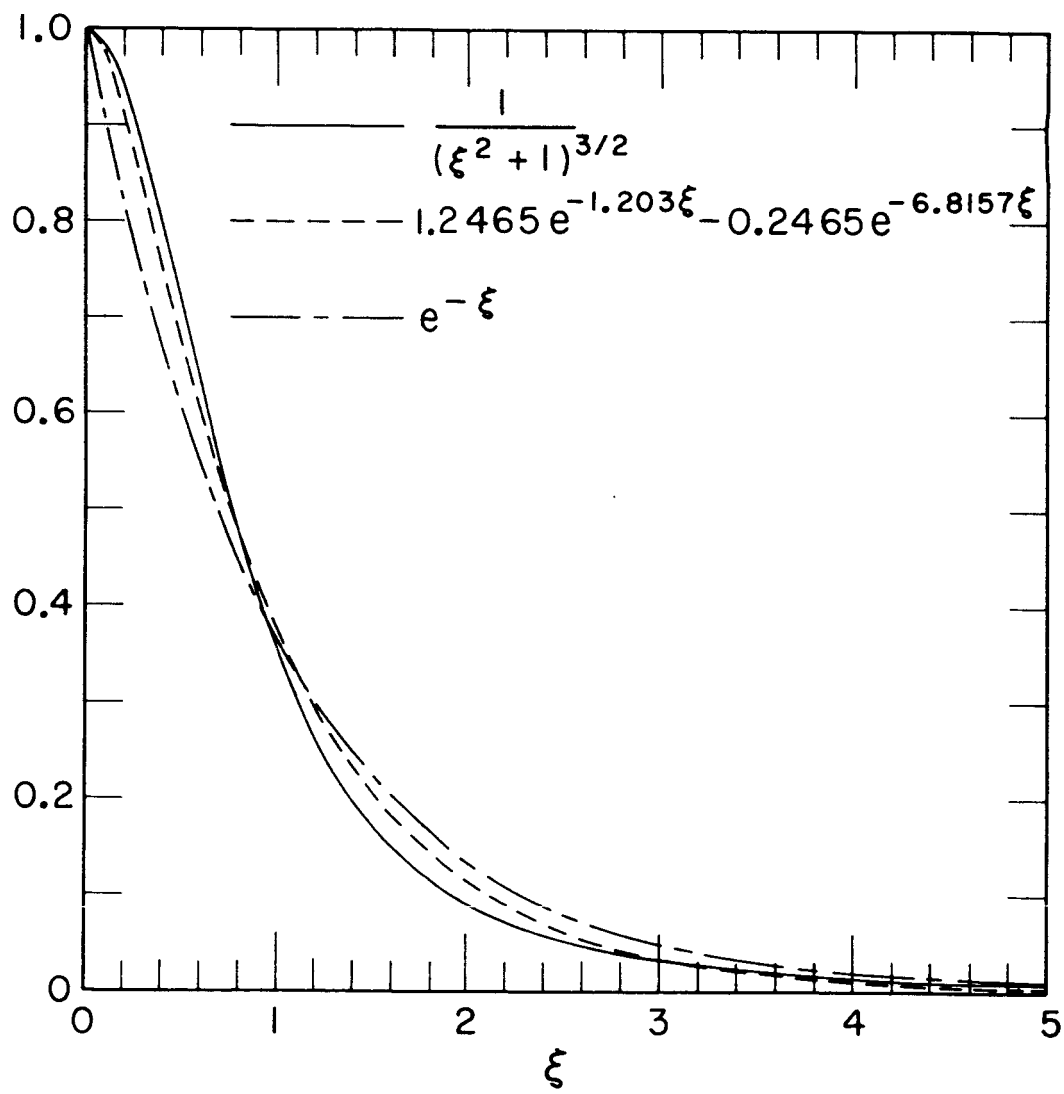


Fig. 6 Variation of Angle Factor with Distance

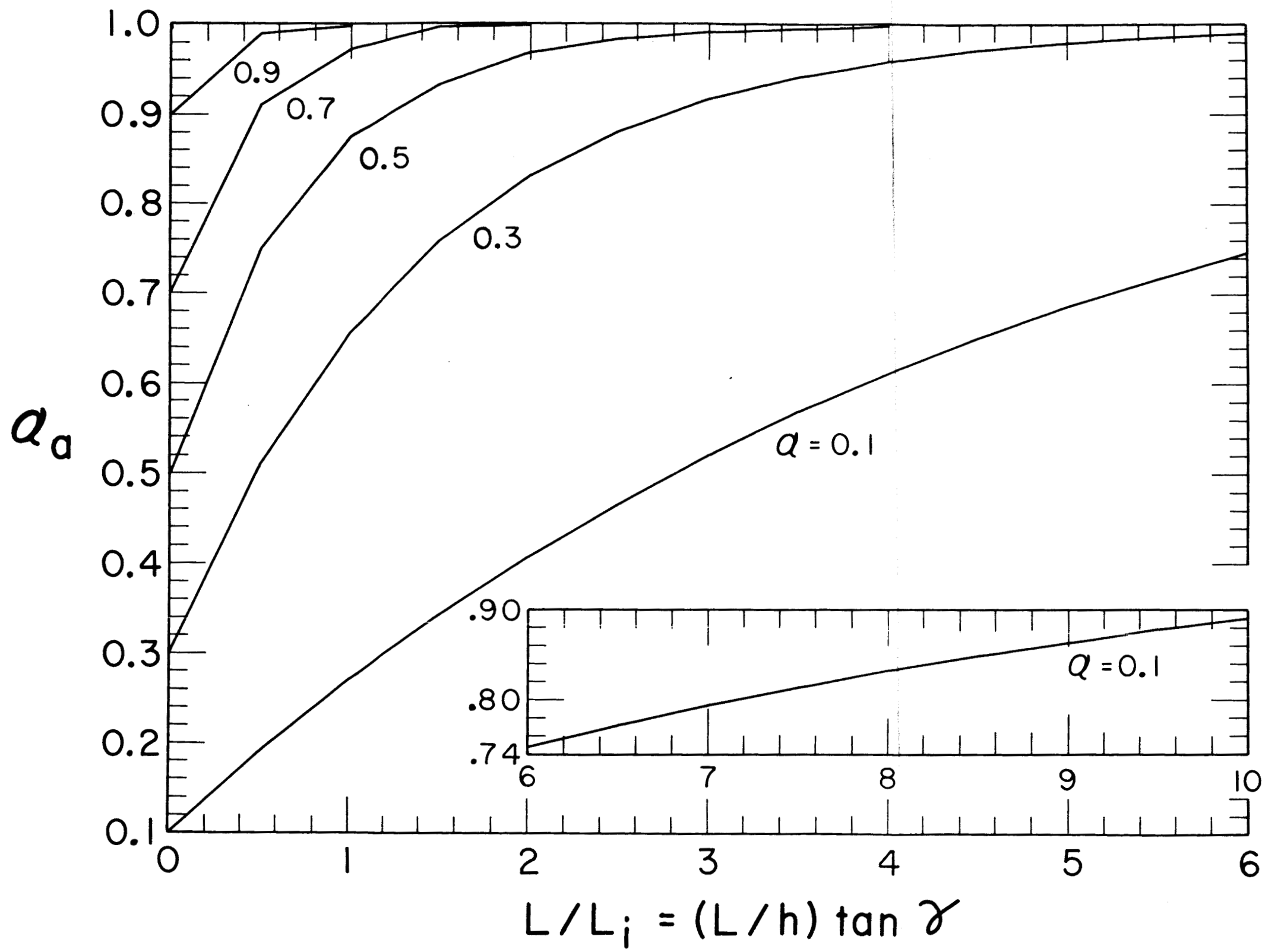


Fig. 9 Apparent Absorptivity for Incoming Parallel Rays in a Diffuse Cavity

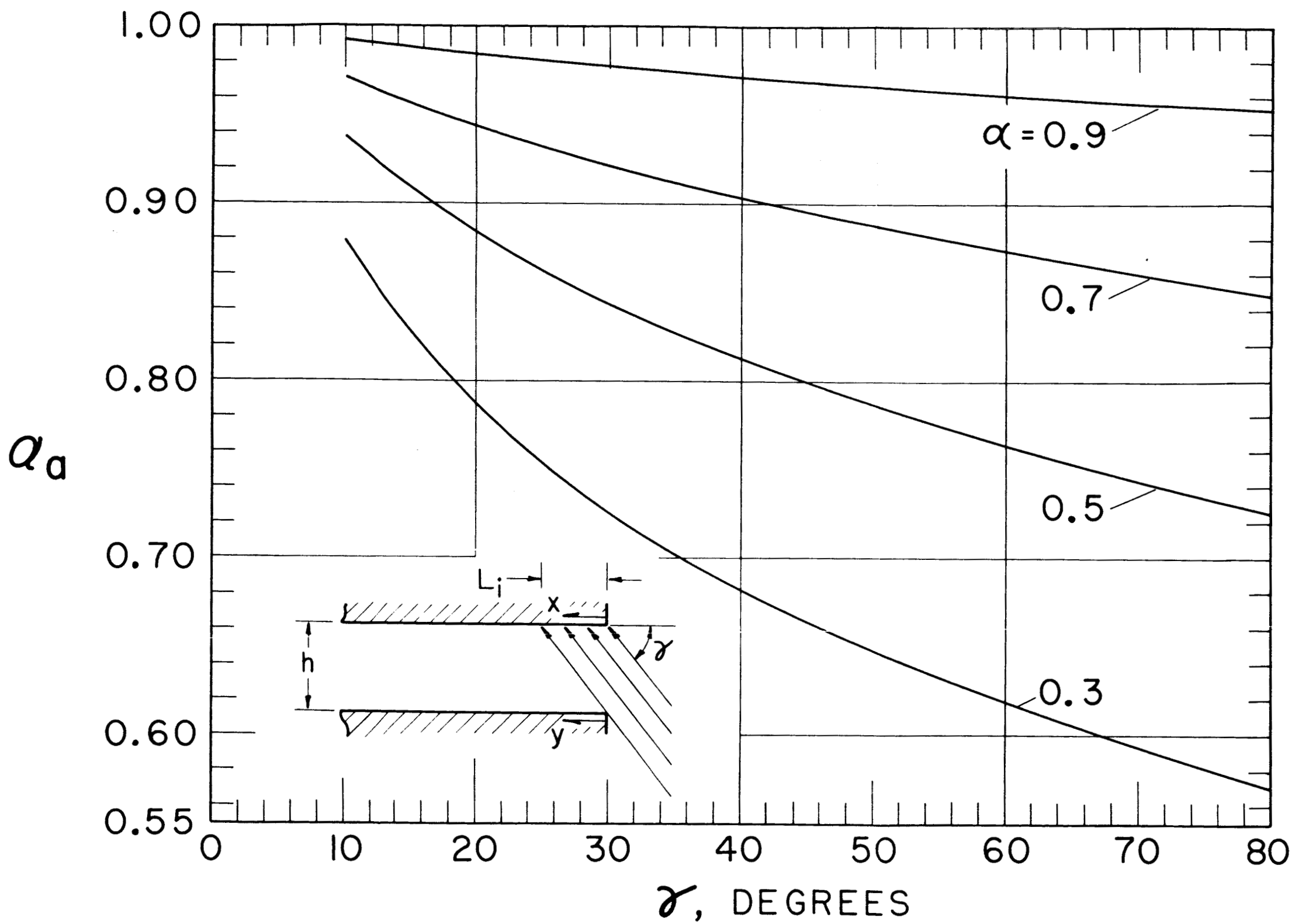


Fig. 5 Apparent Absorptivity for Incoming Parallel Rays in a Diffuse Cavity

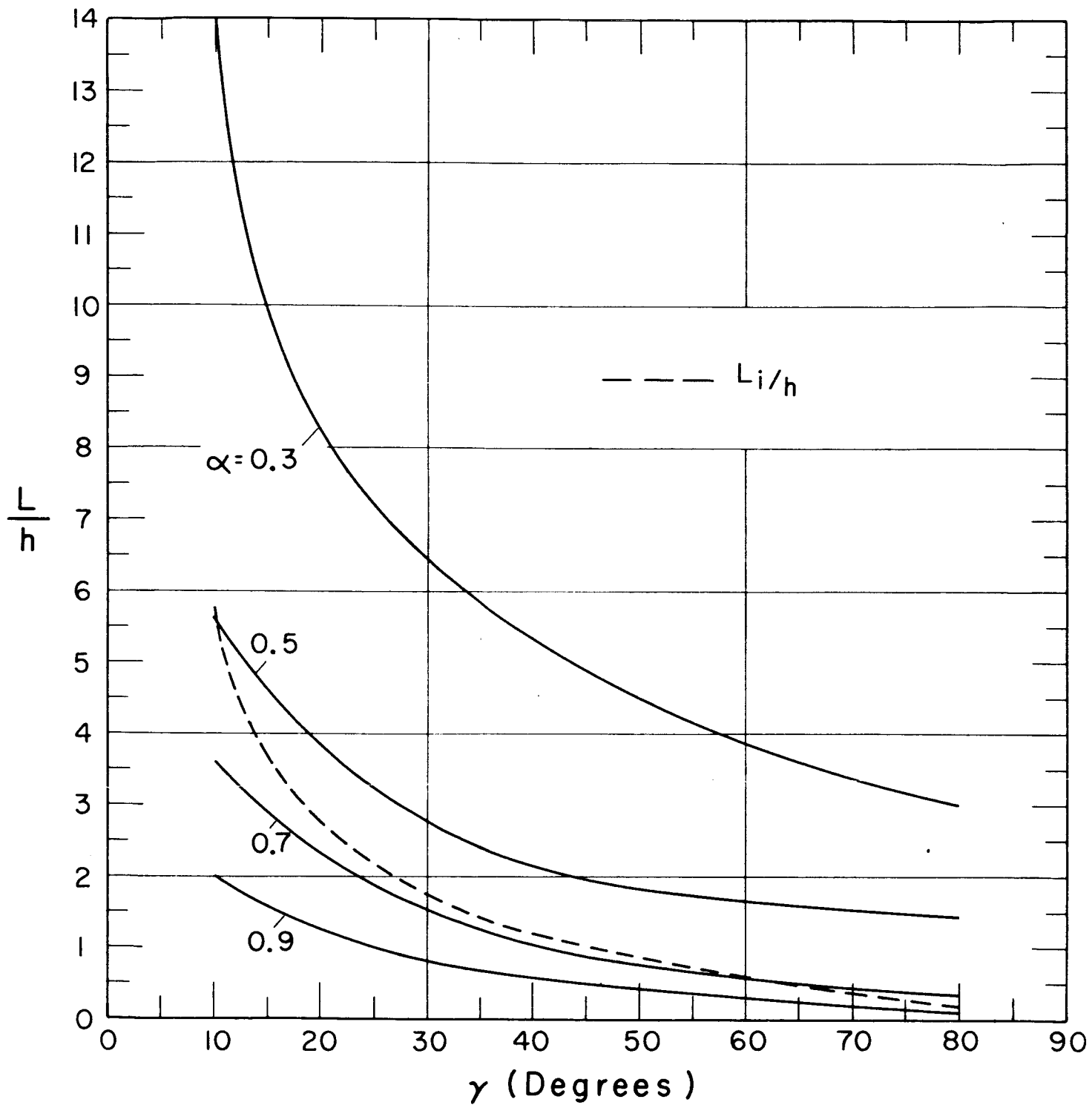


Fig. 7 Aspect Ratio of Finite Cavity at Which Infinite Cavity Results Apply Within 2 Per Cent

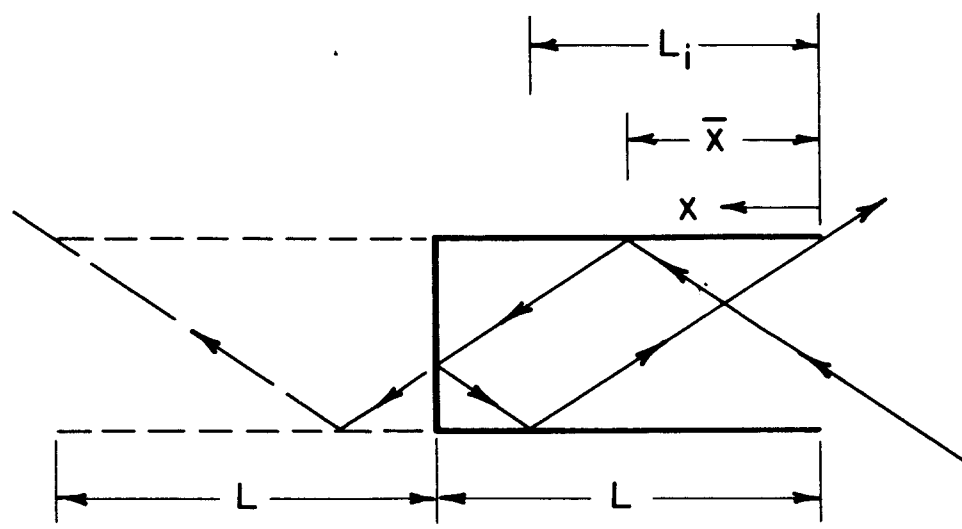


Fig. 8 Incoming Parallel Rays in a Specular Cavity

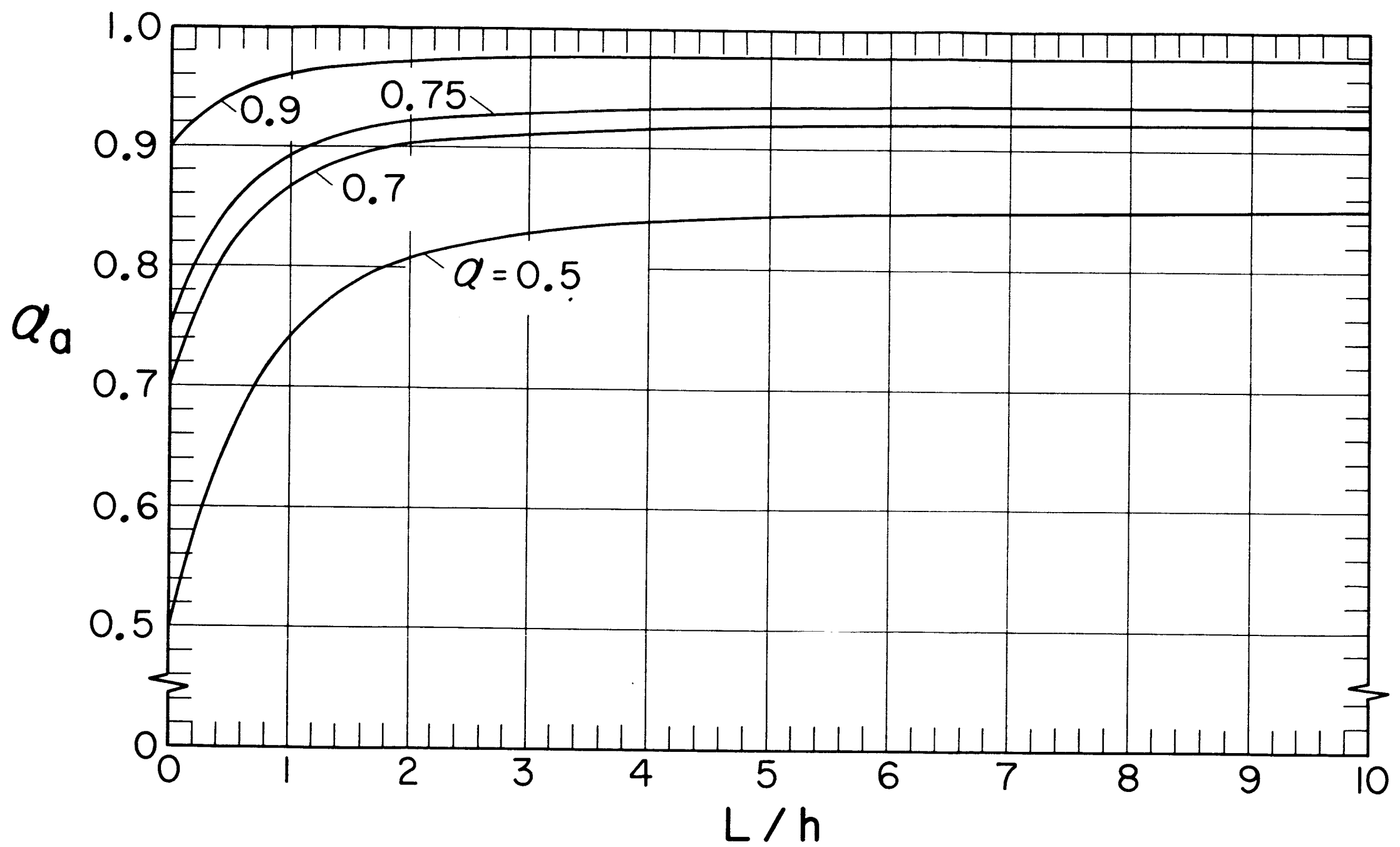
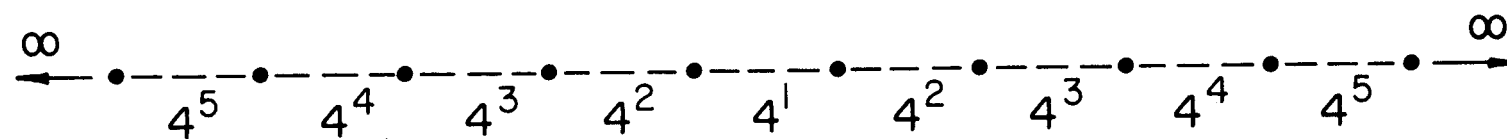
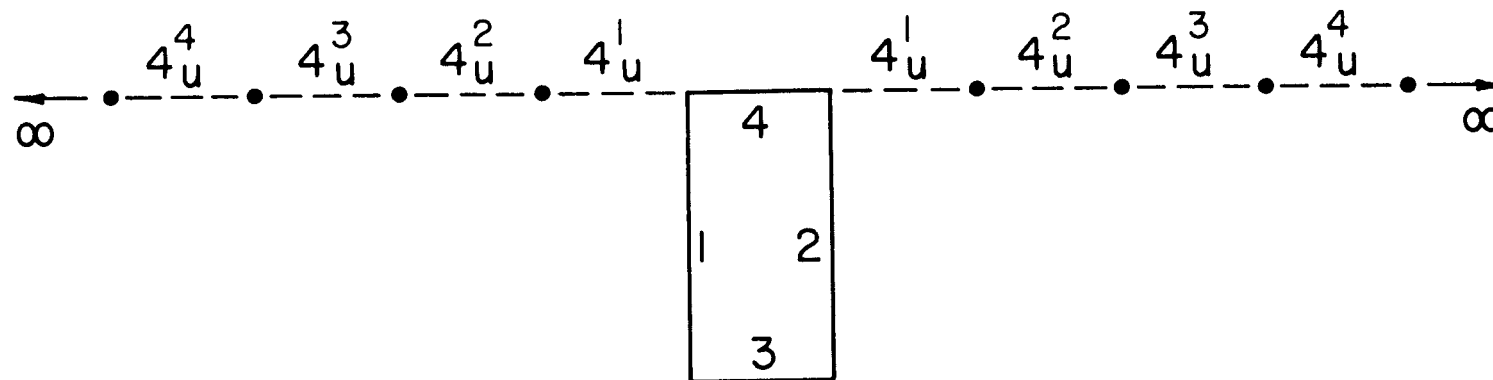


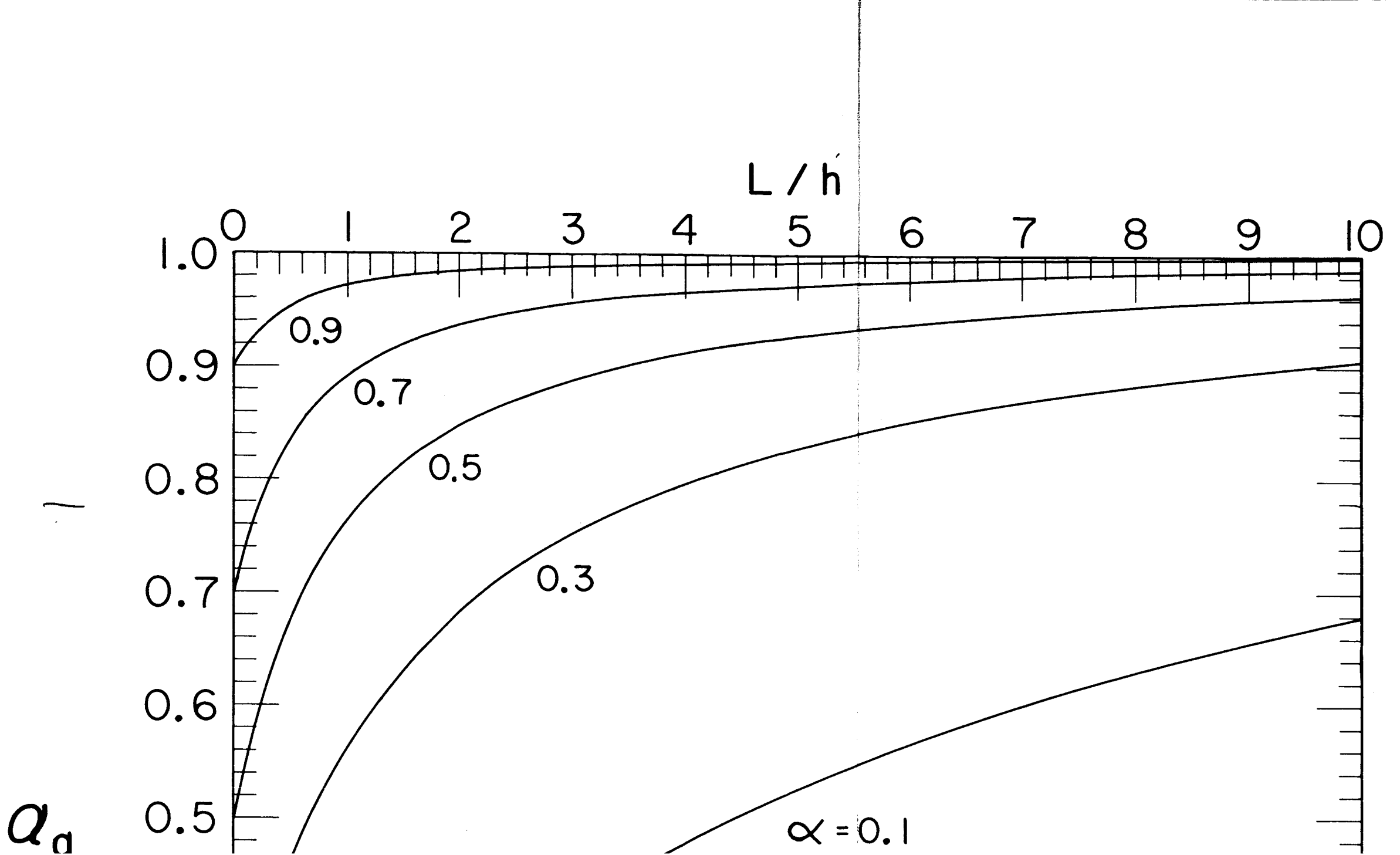
Fig. 2 Apparent Absorptivity for Diffuse Energy Entering a Diffuse Cavity



1, 2, 3: SPECULAR

4: DIFFUSE(BLACK)

Fig. 3 Images Formed by Diffuse Incoming Radiation in a Specular Cavity



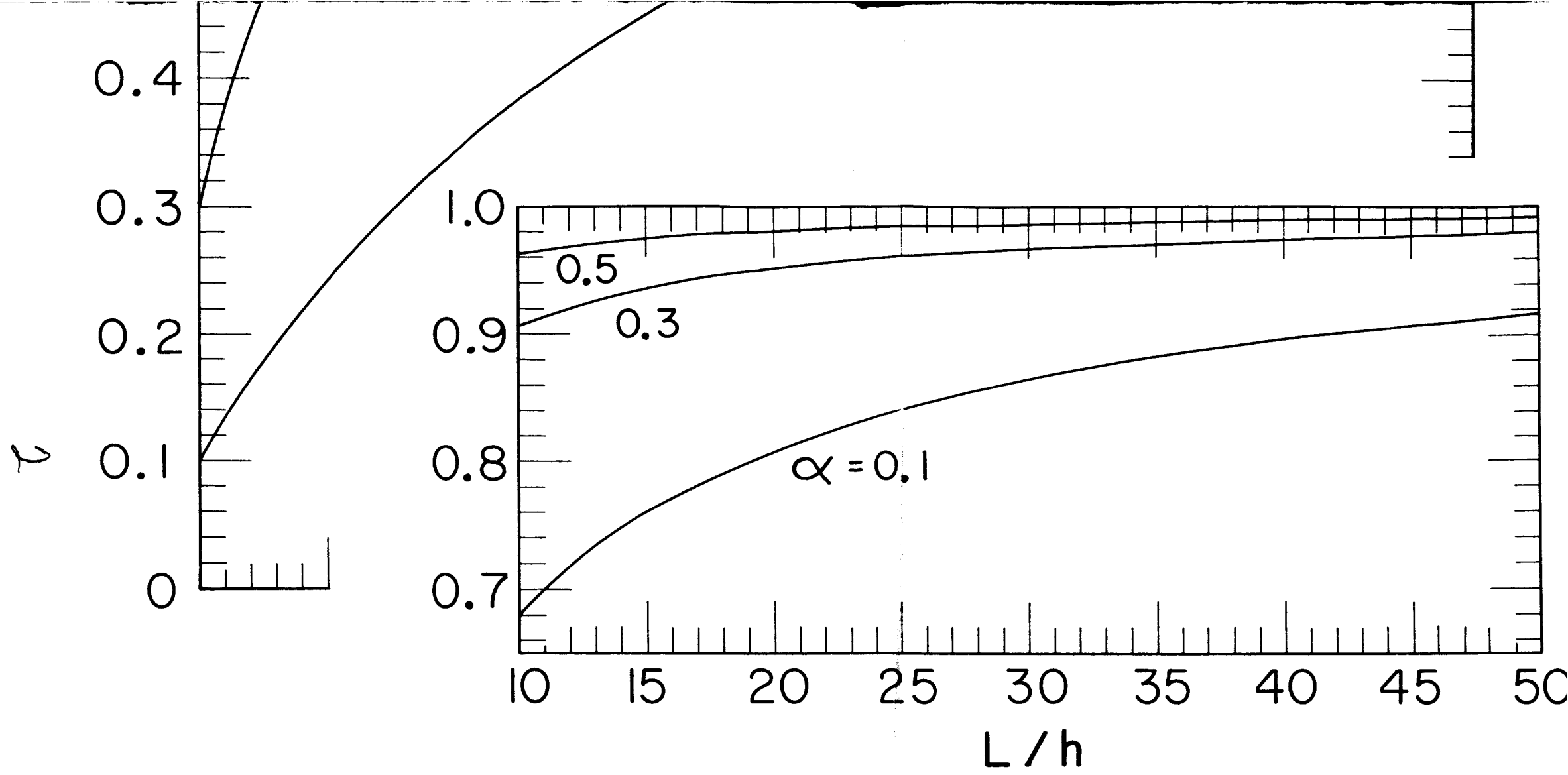


Fig. 4 Apparent Absorptivity for Diffuse Energy Entering a Specular Cavity

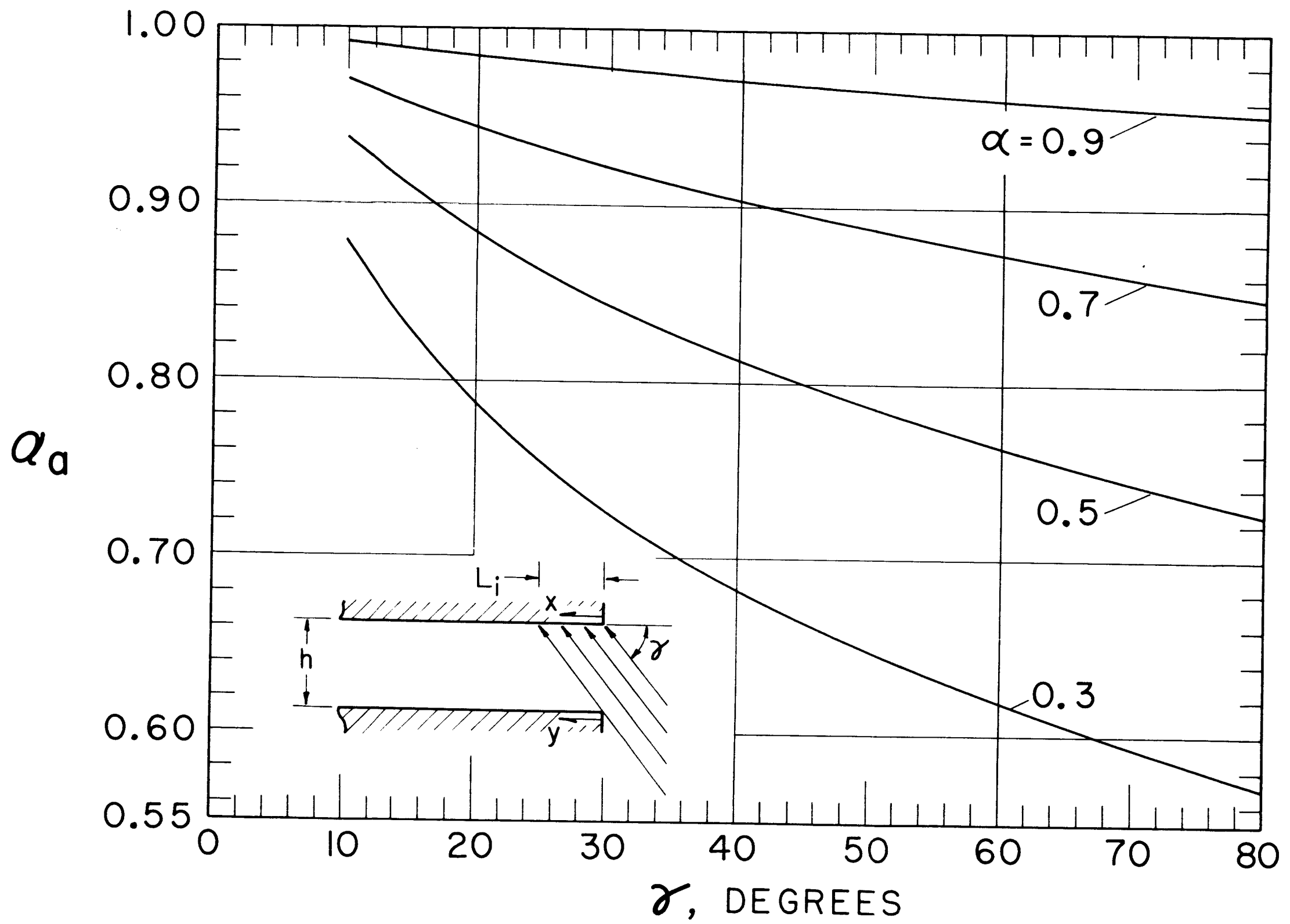


Fig. 5 Apparent Absorptivity for Incoming Parallel Rays in a Diffuse Cavity

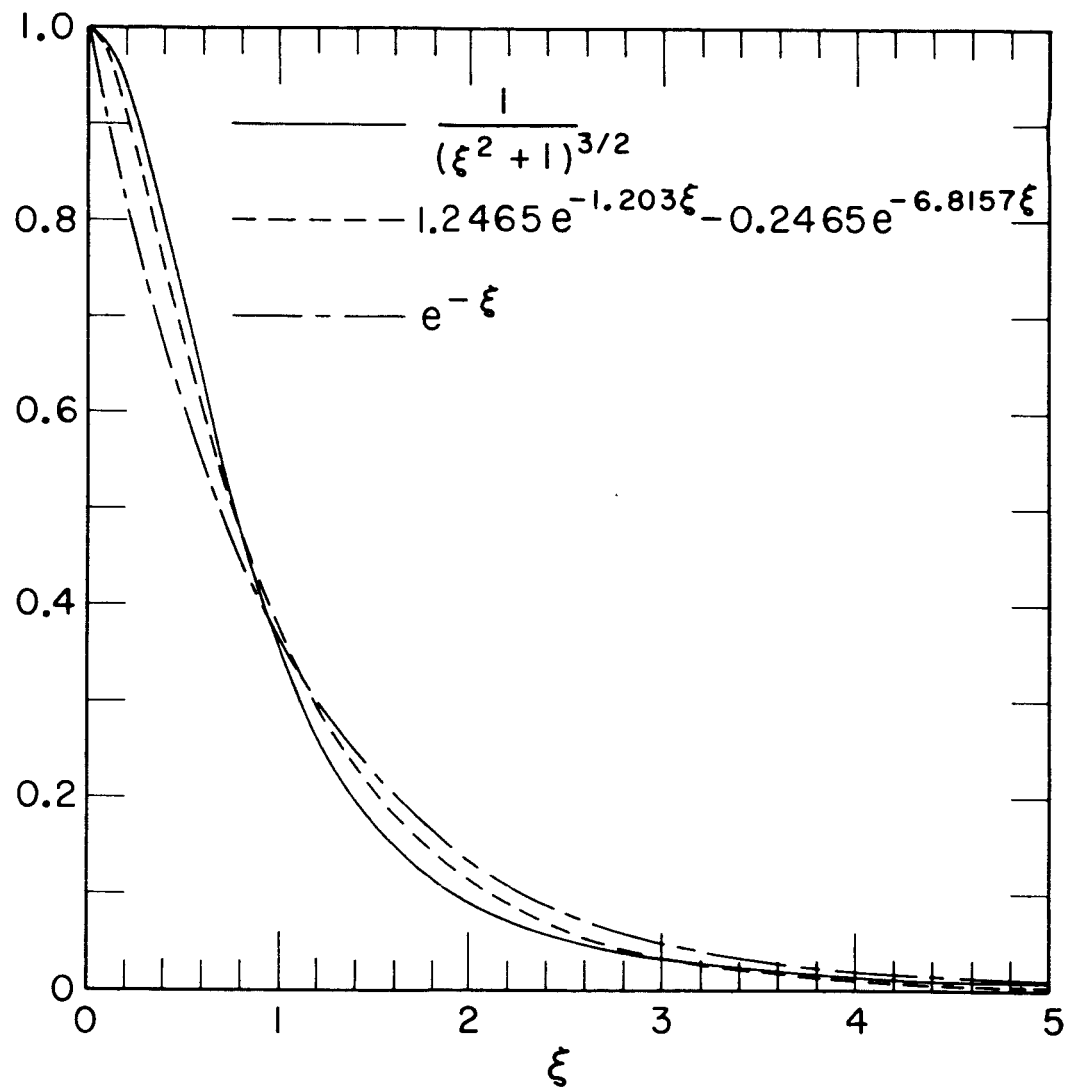


Fig. 6 Variation of Angle Factor with Distance

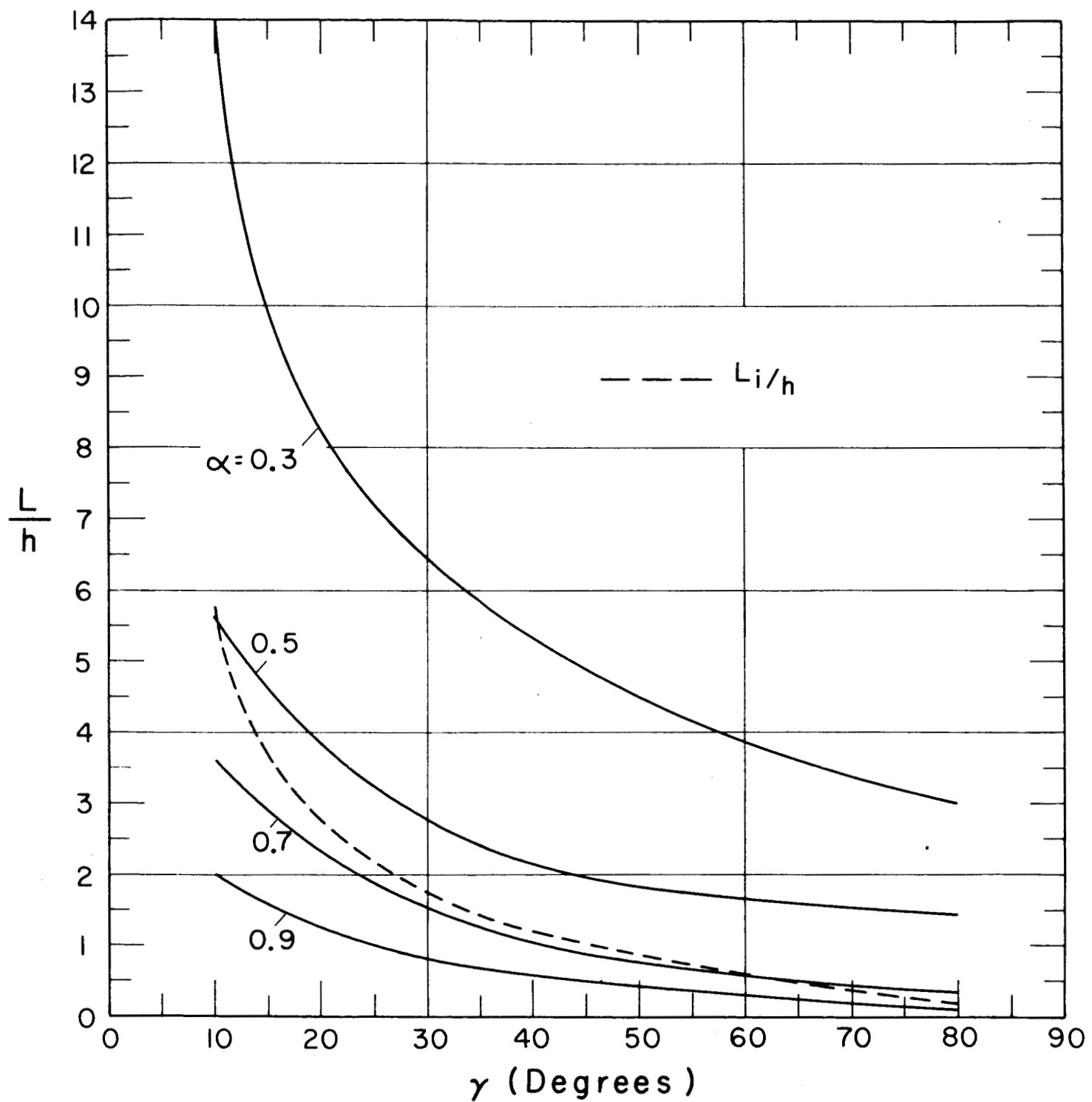


Fig. 7 Aspect Ratio of Finite Cavity at Which Infinite Cavity Results Apply Within 2 Per Cent

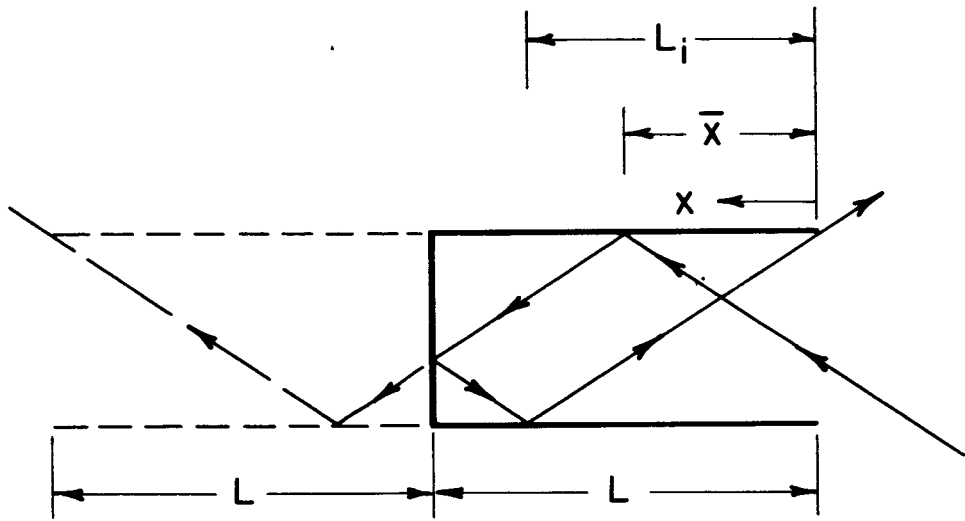


Fig. 8 Incoming Parallel Rays in a Specular Cavity

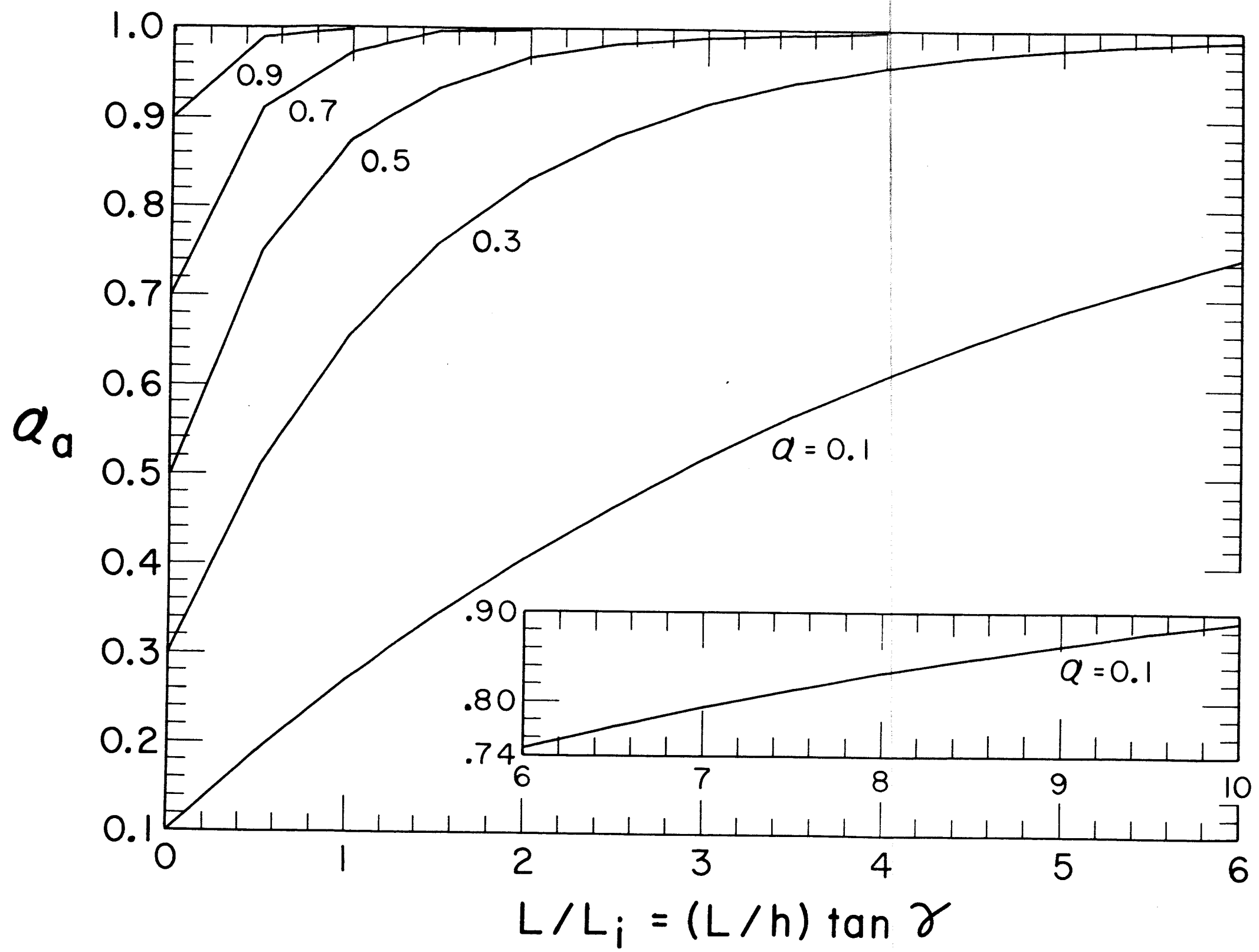


Fig. 9 Apparent Absorptivity for Incoming Parallel Rays in a Diffuse Cavity